Rhodopsin dimers in native disc membranes

Neat rows of paired photon receptors are caught on camera in their natural state.

In vertebrate retinal photoreceptors, the rod outer-segment disc membranes contain densely packed rhodopsin molecules for optimal light absorption and subsequent amplification by the visual signalling cascade[1], but how these photon receptors are organized with respect to each other is not known. Here we use infrared-laser atomic-force microscopy to reveal the native arrangement of rhodopsin, which forms paracrystalline arrays of dimers in mouse disc membranes. The visualization of these closely packed rhodopsin dimers in native membranes gives experimental support to earlier inferences about their supramolecular structure[2,3] and provides insight into how light signalling is controlled.

When activated by a single photon, rhodopsin induces dissociation of the subunits of transducin molecules, which are heterotrimeric G proteins that amplify the light signal. The structure of rhodopsin, which has been solved[4], indicates that it is a prototypical member of subfamily A of G-protein-coupled receptors (GPCRs), which represents about 90% of all GPCRs. The oligomerization[2] of these GPCRs may be important for their own regulation and for interaction with their cognate G proteins.

The probability of single-photon absorption by rhodopsin molecules is increased by their packing arrangement on the tightly stacked rod outer-segment disc membranes[5]. To investigate this organization of rhodopsin, we isolated rod outer-segment disc membranes from mouse retinae, using a protocol that preserves the full biological activity and organization of rhodopsin in the lipid membrane[6] (Y.L. *et al.*, manuscript submitted).

Atomic-force microscopy revealed single-layered disc membranes that were 7–8 nm thick and circular in shape (diameter, 0.9–1.5 μm). Occasionally, complete discs with two stacked membranes were also seen; the thickness of these was 16–17 nm. The most frequently observed surface type (Fig. 1, region 1) was 7.8 ± 0.2 nm thick ($n = 55$) and had a markedly textured topography consisting of densely packed lines. Lipid bilayers had an unstructured topography (Fig. 1, region 2), a height of 3.7 ± 0.2 nm ($n = 86$), and were often seen at the borders of disc membranes. The mica support (Fig. 1, region 3) had no structural features, as expected.

The highly textured surface was assigned as cytoplasmic in view of its relative stiffness. At high magnification, the topography (Fig. 2a, c) revealed rows of rhodopsin pairs densely packed in paracrystalline arrays. Packing densities were 30,000–55,000 rhodopsin monomers per μm^2, with an average density of $48{,}300 \pm 8{,}300$ monomers per μm^2.

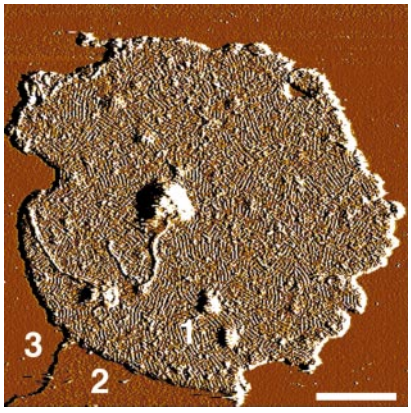

Figure 1 Deflection image of a native eye-disc membrane adsorbed on mica, visualized by atomic-force microscopy (Nanoscope Multimode, Digital Instruments). Three different surface types are evident: 1, the cytoplasmic side of the disc membrane; 2, lipid; and 3, mica. To avoid the formation of opsin, the chromophore-depleted form of rhodopsin[6], membrane samples were never exposed to light. After adsorption of osmotically shocked disc membranes onto mica, their topography was measured in buffer solution (20 mM Tris–HCl (pH 7.8), 150 mM KCl and 25 mM $MgCl_2$). Scale bar, 200 nm.

We deduced the dimensions of the rhodopsin pairs from the angularly averaged powder-diffraction pattern (Fig. 2a, inset, and b, arrows): the innermost arc peaks at $(8.4\ nm)^{-1}$, which results from regularly packed double rows of protrusions; the next ring, at $(4.2\ nm)^{-1}$, reflects the second-order of the double-row repeat, and the axial repeat of the paired rhodopsins that form these rows yields a third ring at $(3.8\ nm)^{-1}$. From real space measurements, we found the distance between the protrusions within each pair to be 3.8 ± 0.2 nm ($n = 40$) and the angle between the lattice vectors to be $85 \pm 2°$ ($n = 8$).

From these dimensions, the highest possible packing density is 62,900 rhodopsin monomers per μm^2. At higher magnification (Fig. 2c), it can be seen that almost all rhodopsin molecules are present in rows of dimers, with a few monomers and some single rhodopsin pairs that have broken away from the rows. This direct demonstration of distinct, densely packed rows of dimers at high resolution is consistent with the proposed dimeric form of native GPCRs that has been inferred from biochemical and pharmacological analysis[2] and from evolutionary trace analysis[3].

The oligomeric organization of GPCR signalling molecules has important implications for G-protein recognition, binding kinetics, signal amplification and signal termination. The shape and dimensions of the paracrystalline unit cell set stringent boundaries for the dimer configuration, the

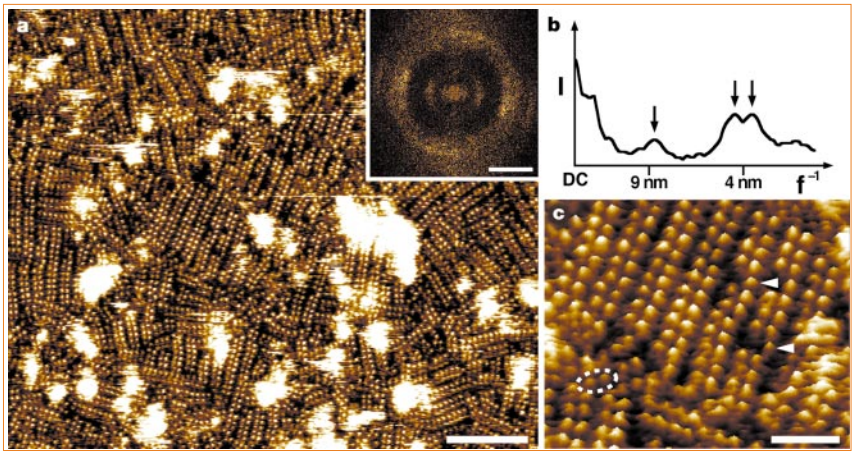

Figure 2 Organization and topography of the cytoplasmic surface of rhodopsin. **a,** Topograph obtained using atomic-force microscopy, showing the paracrystalline arrangement of rhodopsin dimers in the native disc membrane. Inset, arcs in the calculated powder-diffraction pattern reflect the regular arrangement of rhodopsin in the membrane. **b,** Angularly averaged powder-diffraction pattern, showing peaks at $(8.4\ nm)^{-1}$, $(4.2\ nm)^{-1}$ and $(3.8\ nm)^{-1}$. **c,** Magnification of a region of the topograph in **a**, showing rows of rhodopsin dimers, as well as individual dimers (inside dashed ellipse), presumably broken away from one of the rows, and occasional rhodopsin monomers (arrowheads). The rhodopsin molecules protrude from the lipid bilayer by 1.4 ± 0.2 nm ($n = 111$). The topograph in **c** is shown in relief, tilted by 5°. Vertical brightness ranges: 1.6 nm (**a** and **c**). Scale bars: **a**, 50 nm; inset, $(5\ nm)^{-1}$; **c**, 15 nm.

intra-dimer contacts and the formation of oligomers that consist of greater numbers of units (Protein Data Bank accession number, 1N3M).

Dimitrios Fotiadis*, Yan Liang†, Sławomir Filipek‡, David A. Saperstein†, Andreas Engel*, Krzysztof Palczewski†§||

**M. E. Müller Institute for Microscopy, Biozentrum, University of Basel, Basel 4056, Switzerland*

Departments of †Ophthalmology, §Pharmacology and ||Chemistry, University of Washington, Seattle, Washington 98195, USA

e-mail: palczews@u.washington.edu

‡International Institute of Molecular and Cell Biology, and Department of Chemistry, University of Warsaw, Warsaw 02-109, Poland

1. Papermaster, D. S. *Invest. Ophthalmol. Vis. Sci.* **43,** 1300–1309 (2002).
2. Rios, C. D., Jordan, B. A., Gomes, I. & Devi, L. A. *Pharmacol. Ther.* **92,** 71–87 (2001).
3. Dean, M. K. *et al. J. Med. Chem.* **44,** 4595–4614 (2001).
4. Palczewski, K. *et al. Science* **289,** 739–745 (2000).
5. Molday, R. S. *Invest. Ophthalmol. Vis. Sci.* **39,** 2491–2513 (1998).
6. McBee, J. K., Palczewski, K., Baehr, W. & Pepperberg, D. R. *Progr. Retin. Eye Res.* **20,** 469–529 (2001).

Competing financial interests: declared none.

Coulomb fission

Rayleigh jets from levitated microdroplets

Electrified droplets are generated in thunderstorm clouds, as well as in technological applications such as ink-jet printing and electrospray ionization, but they become unstable when charged beyond the Rayleigh limit[1]. Here we record the dynamics of the disintegration process by examining levitated droplets under high-speed microscopy. These images may help to explain one of the oldest unsolved problems in experimental and theoretical physics.

Lord Rayleigh showed that the spherical shape of a drop of radius a_0, surface tension σ and charge Q, remains stable as long as the fissility $X = Q^2/(64\pi^2\epsilon_0\sigma a_0^3)$ does not exceed unity[1]. As X approaches unity, the quadrupole deformation is the first to become unstable; when X increases beyond unity, however, an instability occurs that is associated with the formation of fine jets (known as Rayleigh jets) "whose fineness, however, has a limit"[1]. Although this conjecture has since been examined both experimentally[2–4] and theoretically[5,6], the mechanics of the break-up of these charged droplets and the details of the jets' fineness remain unclear.

We used high-speed microscopic images to observe the disintegration of droplets charged to the Rayleigh limit and the production of Rayleigh jets. In our experimental set-up, a charged droplet of ethylene glycol is produced by using a piezo-driven nozzle and is suspended in an electrodynamic levitator; the droplet is illuminated by an unfocused He–Ne laser and the mass/charge ratio and the radius of the droplet are determined in real time by analysis of the scattered light[7,8].

At the moment of injection, the droplet radius, a_0, is 58 μm and its charge is about 3.3 picocoulombs. It subsequently shrinks through evaporation of neutral molecules, reaching the Rayleigh limit of stability at a radius of about 24 μm. Just before this point, the amplitude of the quadrupole-shaped oscillation of the droplet increases drastically[9], triggering a signal to a fast flashlamp that fires after a predefined delay, Δt, and is recorded by a digital microscope as a still image of the droplet. This process is repeated with subsequent droplets, using increasing delay times.

These microscopic images of the disintegration process of our levitated microdroplets are reproduced in Fig. 1a–f. During the first 150 μs, the droplet stretches from a sphere into an ellipsoid, as predicted by Rayleigh (Fig. 1a). It then develops two sharp tips on the poles of the ellipsoid (Fig. 1b). Almost instantaneously after tip formation, a fine jet of liquid is ejected from both tips in opposite directions (Fig. 1c). This jet later disintegrates into fine droplets (Fig. 1d) that are repelled from the mother droplet by Coulomb repulsion. The tip edges disappear after the ejection of the jet (Fig. 1e), and the barrel-shaped parent droplet then contracts until it regains spherical symmetry after about 210 μs (Fig. 1f).

During the jet's disintegration, roughly 100 small daughter droplets are formed, which carry 33% of the total charge and constitute about 0.3% of the mass of the mother droplet. The diameter of the jet is determined from higher-resolution images to be 1.5 μm: the droplets generated during disintegration are of roughly the same size and are themselves close to a fissility of $X_{\mathrm{frag}} = 1$ and so presumably undergo a Rayleigh instability soon afterwards.

As this behaviour is independent of the levitator voltage, we argue that it must correspond closely to that of free, highly charged droplets. But, in contrast to Lord Rayleigh's prediction, we observed the jets at a fissility of unity, indicating that renewed investigation will be necessary to explain the complex hydrodynamics of this century-old problem.

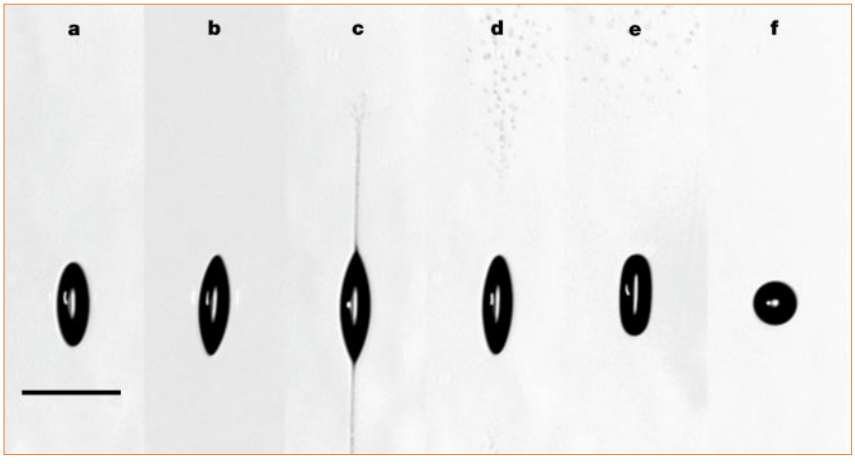

Figure 1 High-speed imaging of the disintegration of a levitated droplet charged to the Rayleigh limit. The droplet (radius, 24 μm) is imaged on a vertical charge-coupled-device array to determine and control its vertical position in the levitator, and on a photomultiplier that detects instability-onset, quadrupole-shaped oscillations of the droplet. These oscillations trigger a signal to a flashlamp that fires after a predefined delay, Δt. The image is observed through a microscope with a long working distance (Mitutoyo). **a–f,** Microscopic images taken at Δt values (in μs) of: **a**, 140; **b**, 150; **c**, 155; **d**, 160; **e**, 180, and **f**, 210. The droplet changes from a sphere to an ellipsoid (**a**), tips appear at the poles (**b**) and a fine jet of liquid is ejected from each tip (**c**); the jets disintegrate (**d**) and the elliptical droplet reassumes a spherical shape (**e**, **f**). Further experimental details are available from the authors. Scale bar, 100 μm.

Denis Duft, Tobias Achtzehn, Rene Müller, Bernd A. Huber*, Thomas Leisner

Institut für Physik, Technische Universität Ilmenau, Postfach 100565, 98684 Ilmenau, Germany

e-mail: thomas.leisner@TU-Ilmenau.de

**Permanent address: Centre Interdisciplinaire de Recherche Ions Lasers, rue Claude Bloch, 14070 Caen Cedex 5, France*

1. Rayleigh, Lord *Phil. Mag.* **14,** 184–186 (1882).
2. Taylor, G. I. *Proc. R. Soc. Lond. A* **280,** 383–397 (1964).
3. Smith, J. N., Flagan, R. C. & Beauchamp, J. L. *J. Phys. Chem. A* **106,** 9957–9967 (2002).
4. Davis, E. J. & Schweiger, G. *The Airborne Microparticle* (Springer, Heidelberg, 2002).
5. Tsampoulos, J. A., Akylas, T. R. & Brown, R. A. *Proc. R. Soc. Lond. A* **401,** 67–88 (1985).
6. Pashkevich, V. V., Krappe, H. J. & Wehner, J. *Z. Phys. D* **40,** 338–340 (1997).
7. Krämer, B. *et al. J. Chem. Phys.* **111,** 6521–6527 (1999).
8. Schwell, M. *et al. J. Phys. Chem. A* **104,** 6726–6732 (2000).
9. Duft, D., Lebius, H., Huber, B. A., Guet, C. & Leisner, T. *Phys. Rev. Lett.* **89,** 0845031–0845034 (2002).

Competing financial interests: declared none.